NASA Technical Memorandum 83012

Correlation of Core Noise Obtained by Three-Signal Coherence Techniques

U. von Glahn and E. Krejsa
Lewis Research Center
Cleveland, Ohio

Prepared for the
One hundred fourth Meeting of the Acoustical Society of America
Orlando, Florida, November 9–12, 1982

NASA

CORRELATION OF CORE NOISE OBTAINED BY THREE SIGNAL COHERENCE TECHNIQUES

U. von Glahn and E. Krejsa

National Aeronautics and Space Administration
Lewis Research Center
Cleveland, Ohio 44135

E-1447

ABSTRACT

The prediction of frequency content and noise levels of turbofan engine core noise is reexamined as a result of recent test data and a new diagnostic technique (E. A. Krejsa, NASA TM-82634, 1981). The diagnostic technique, utilizing a three-signal coherence method, is used to obtain core noise spectra for several engines. Similarities and differences of the spectra are discussed. Finally, the three-signal coherence data are correlated, leading to an improved core noise prediction procedure.

INTRODUCTION

Of the various noise sources inherent to turbine-powered conventional aircraft, fan and jet noise are generally considered to be the primary noise offenders to the community. As these noise sources are reduced other sources, such as the engine core and the airframe, emerge to provide barriers to further aircraft noise reductions and the ability to meet new or lower noise requirements, whether local, federal, or international (refs. 1 and 2). It has been generally conceded that engine core noise is an important noise source during approach and cutback engine operation. However, it was shown in reference 1, that engine core noise was a significant noise source at full-power conditions, indeed constituting a floor for further aircraft noise reductions for wide body commercial aircraft using high-bypass engines. Documentation of the importance of core noise to the overall high-bypass turbofan engine noise is also given in reference 3 in which core noise was shown to be the dominant noise source between directivity angles of 80 to 130° for a JT9D-7 engine operating at full-power conditions.

On the basis of limited engine core noise data, several core noise prediction procedures were developed (e.g., refs. 4 to 7). These prediction procedures frequently assume that engine core noise spectra peak near 400 to 500 Hz, independent of engine airflow. In references 4 and 7, a variation in peak frequency with engine airflow was included in the prediction formulation. However, beyond a limited range of peak frequencies it was recommended in reference 4 that a constant value of 500 Hz be used.

Recently, a new method was developed that permits the core noise levels from gas turbine engines to be measured directly (ref. 8). The method utilizes a three-signal coherence technique to determine directly the levels of the far-field noise that propagates from the engine core. The technique has been applied to signals measured from three engines: JT15D, YF102, and CF6-50 (refs. 9 to 11). Core noise levels as a function of frequency and radiation angle were measured over a range of engine speeds. These measurements indicate that the prediction procedures of references 4 to 7 are inadequate. In particular, the assumption that the peak frequency is near 400 Hz for all engines appears to be invalid.

In the present study an engine core noise prediction procedure based upon these three-signal coherence analyses is developed. Included in the procedure are considerations of (1) peak spectral noise levels and associated frequencies, (2) spectral shape, and (3) core noise directivity.

CORE NOISE SPECTRAL DIAGNOSTICS

Core noise spectra for the JT15D, YF102, and CF6-50 (refs. 9 to 11) core engines were obtained using the three-signal coherence technique of reference 8. Briefly, this diagnostic technique requires the measurement of fluctuating pressures in the far-field and at two locations within the engine core. For the present work, one core pressure measurement location was in the combustor and the other was in the tailpipe. The cross-spectra of these measurements were used to determine the levels and frequency content of the far-field noise that propagates from the engine core. The technique permits measurement of core noise even when other noise sources dominate the noise field, as in the case of most engines when operating at full power. Furthermore, no knowledge of other noise sources contributing to the far-field noise is required. Details of the technique are given in reference 8.

ANALYSIS

Because the measured spectral data obtained by the three-signal technique indicated several peaks, as will be discussed later, core noise spectra segmentation into one, two-, and four-spectral segments was included in the analysis. The segments were intended to represent the various spectral peaks. Spectral shapes were developed for each of the spectral segments. Note that all sound pressure levels are free field plus 6dB corresponding to the as-measured levels using ground level microphones.

The peak sound pressure level, SPL_p, at $\theta = 120^\circ$ for each spectral segment was plotted as a function of parameters generally considered responsible for combustion/core noise. In the initial analysis these parameters included consideration of variables associated with combustor exit velocities raised to exponents of four, six, and eight and a heat addition model. Additional factors, generally consisting of geometry terms and, in some cases, fluid properties, were then included to account for differences in the core engine configurations.

For each SPL_p, the associated frequency, f_p, was then determined as a function of a modified Strouhal number. The modifications generally consisted of core engine geometry factors.

Finally, overall sound pressure levels, OASPL, were calculated at $\theta = 120^\circ$ for measured data and several spectral models and then compared. On the basis of limited data obtained from the YF102 engine core noise study, the OASPL variation with directivity angle is discussed.

SPECTRAL SHAPE

In general, present core noise prediction procedures assume the core noise spectrum to be a smooth curve. However, as pointed out in reference 8, the core noise spectrum, excluding very high frequency turbine noise, obtained by the three-signal coherence technique exhibits several peaks.

In the present study, several segmentation spectral shapes associated with the spectral peaks are considered. Initially a single-segment spectral shape, as generally assumed in the literature, was generated for the composite available data for the JT15D, YF102, and CF6-50 engines. Spectral shapes consisting of 2 and 4 segments, respectively, were then generated and aimed at matching the several peaks in the measured spectral shapes. The selected spectral shapes are shown in figure 1 in terms of the change in decibels referenced to the peak sound pressure level of the spectral segment, SPL_p, with the associated frequency, f_p. Also shown in the figure are the coordinates for the various spectral shapes.

A comparison of the several spectral shapes of figure 1 with the CF6-50 engine data for an engine speed of 93-percent engine speed is shown in figure 2. It is apparent that multisegment spectra fit the measured data better than a single-segment spectrum. The curves shown in figure 2 do not include the increased sound pressure levels (up to 3 dB) normally associated with the intersection of two spectra.

SEGMENT PEAK SOUND PRESSURE LEVEL

The peak sound pressure levels of the various segmented spectra when plotted as functions of several correlation parameters were best correlated in terms of a combustor exit velocity with an exponent of 4.0 (V_c^4) in the low frequency range and a heat addition parameter in the high frequency range. The latter parameter is given in references 6 and 12. However, for each spectral segment additional geometry and/or fluid property factors also had to be included.

The following section summaraizes the segment peak sound pressure level, SPL_p, correlations developed in this study. All data shown are for a directivity angle, θ, of 120°. All levels are free field plus 6dB.

ONE-SEGMENT SPECTRUM

For a single-segment noise spectrum, the peak sound pressure level could best be correlated on the basis of a heat release parameter given in previous correlations (refs. 6 and 12) by

$$SPL_p \sim 10 \log w \left(\frac{P_c}{P_a} \frac{\Delta T_c}{T_{c,i}} \right)^2 \qquad (1)$$

Equation (1) correlated the SPL_p values for the JT15D and YF102 core engines on a single curve. However, the CF6-50 core engine SPL_p values, while correlated with equation (1), were displaced from the small engine data. In reference 5, the design point (or take-off power) temperature drop across the turbine was used to correlate the noise levels for various engine types. However, for the present three turbofan engines such a parameter would separate the JT15D data from the YF102 data. At the same time the CF6-50 data could be correlated with one or the other of the two small engines but not both.

The CF6-50 engine utilizes an annular-plug-type exhaust nozzle, whereas the two smaller engines utilize circular exhaust nozzles. Consequently, a geometry parameter, D_h/D_e, was selected to correlate all the SPL_p values on a common curve. (Note that D_h/D_e for the JT15D and YF102 core engines is 1.0). The SPL_p values as a function of these variables are shown in figure 3. An equation expressing this relationship is given as follows:

$$SPL_p = 91 + 10 \log w \left(\frac{P_c}{P_a} \frac{\Delta T_c}{T_{c,i}}\right)^2 \left[\left(\frac{D_h}{D_e}\right)^4\right] - 20 \log R \qquad (2)$$

TWO-SEGMENT SPECTRUM

The development of a two segment spectrum requires a separate correlation of the SPL_p for each segment.

Spectral segment I, low frequency. - The low frequency segment, SPL_p, of the spectrum (< 200 Hz) could best be correlated with the combustor exit velocity with an exponent of 4.0 and modified by both fluid stream and geometry factors. The variation of the measured $SPL_{p,I}$ with these parameters is shown in figure 4(a). An equation expressing this relationship is given by

$$SPL_{p,I} = 67.5 + 10 \log \rho_c A_c \frac{V_c^4}{C_a} \left[\left(\frac{\rho_c}{\rho_a}\right)^2 \left(\frac{D_c}{D_e}\right)^4 \left(\frac{D_h}{D_e}\right)\right] - 20 \log R \qquad (3)$$

where subscript I refers to the low frequency spectral segment.

Spectral segment II, high frequency. - The high frequency segment, SPL_p(> 200 Hz), was best represented by the same heat-release parameter and acoustic transmission-loss factor used for the single-segment spectrum, except that the constant is 89 instead of 91. Thus, $SPL_{p,II}$ is expressed by

$$SPL_{p,II} = 89 + 10 \log w \left(\frac{P_c}{P_a} \frac{\Delta T_c}{T_{c,i}}\right)^2 \left[\left(\frac{D_h}{D_e}\right)^4\right] - 20 \log R \qquad (4)$$

The variation of measured $SPL_{p,II}$ with the preceding modified heat-release parameter is shown in figure 4(b).

FOUR-SEGMENT SPECTRUM

As in the preceding spectrum development, the four segment spectrum requires a separate SPL_p correlation for each segment.

Spectral segments I and II, low frequency. - In general for the three engines included herein, the low (< 200 Hz) and high (> 200 Hz) frequency SPL ranges were each divided into two spectral segments. As in the preceding two-segment spectrum, the low frequency segments I and II

were correlated using V_c^4 modified for fluid properties and geometry factors. The high frequency segments III and IV were again correlated by a modified heat addition parameter. The correlated measured SPL_p for each of the four spectral segments are shown in figure 5. Equations expressing these relationships are as follows:

$$SPL_{p,I} = 48.0 + 10 \log \rho_c A_c \frac{V_c^4}{C_a} \left[\left(\frac{\rho_c}{\rho_a}\right)^2\right] - 20 \log R \quad (5)$$

$$SPL_{p,II} = 68.5 + 10 \log \rho_c A_c \frac{V_c^4}{C_a} \left[\left(\frac{\rho_c}{\rho_a}\right)^2 \left(\frac{D_c}{D_e}\right)^4 \left(\frac{D_h}{D_e}\right)^2\right] - 20 \log R \quad (6)$$

$$SPL_{p,III} = 90.0 + 10 \log w \left(\frac{P_c}{P_a} \frac{\Delta T_c}{T_{c,i}}\right)^2 \left[\left(\frac{D_h}{D_e}\right)^4\right] - 20 \log R \quad (7)$$

$$SPL_{p,IV} = 73.5 + 10 \log w \left(\frac{P_c}{P_a} \frac{\Delta T_c}{T_{c,i}}\right)^2 \left[\left(\frac{D_h}{D_c}\right)^2 \left(\frac{D_h}{D_e}\right)^5\right] - 20 \log R \quad (8)$$

SEGMENT PEAK FREQUENCY

In order to correlate the frequency, f_p, at which the sound pressure level peaked for each spectral segment, a Strouhal dependency modified by geometry factors was utilized. The resultant equations for the various segment peak frequencies are given in the following section

ONE-SEGMENT SPECTRUM

$$f_p = 0.083 \frac{V_c}{D_c} \left[\left(\frac{C_c}{C_a}\right)^{0.5} \left(\frac{D_h}{D_c}\right) \left(\frac{D_e}{D_c}\right)^{0.5}\right] \quad (9)$$

TWO-SEGMENT SPECTRUM

$$f_{p,I} = 0.025 \frac{C_c}{D_c} \left[\left(\frac{C_c}{C_a}\right) \left(\frac{D_h}{D_e}\right)^{0.75}\right] \quad (10)$$

The form of equation (10) is somewhat analogous to that given for combustion noise in reference 13.

$$f_{p,II} = 0.25 \left[\frac{V_c}{D_c} \left(\frac{D_e}{D_c}\right) \left(\frac{D_h}{D_e}\right)^{0.5}\right] \quad (11)$$

FOUR-SEGMENT SPECTRUM

$$f_{p,I} = 0.06 \frac{V_c}{D_c} \left[\left(\frac{D_e}{D_c} \right)^{0.5} \left(\frac{D_e}{D_h} \right)^{0.25} \right] \quad (12)$$

$$f_{p,II} = 0.09 \frac{V_c}{D_c} \left[\left(\frac{C_c}{C_a} \right) \left(\frac{D_e}{D_h} \right)^{0.5} \right] \quad (13)$$

$$f_{p,III} = 0.25 \frac{V_c}{D_c} \left[\left(\frac{D_e}{D_c} \right) \right] \quad (14)$$

$$f_{p,IV} = 0.75 \frac{V_c}{D_c} \left[\left(\frac{D_e}{D_c} \right) \right] \quad (15)$$

The validity, i.e., goodness, of equations (9) to (15) is demonstrated in the comparison of the measured and predicted spectra shown in the figures discussed in the next section.

COMPARISON OF MEASURED SPECTRA WITH CORRELATION SPECTRA

By utilizing the correlations of SPL_p, f_p, and the segmented spectral shapes developed in the preceding sections, empirical core noise spectra were constructed and compared with measured spectra obtained by use of the three-signal coherence technique. These comparisons are shown in figures 6, 7, and 8 for the JT15D, YF102, and CF6-50 core engines, respectively. As previously noted, the curves shown do not include the increased sound pressure levels normally associated with the intersection of two spectra.

As expected, the four-segment spectrum provides the best overall fit to the measured data, with the single-segment spectrum providing the poorest fit. Also the constructed spectra indicate that with a single-segment spectrum, the frequency at the peak sound pressure level for all three engines is generally significantly less than the commonly quoted 400 to 500 Hz in the literature.

The two-segment spectrum appears to be a reasonable representation of the combustion noise. The high frequency segment for the JT15D, YF102, and CF6-50 core engines occurs in the 400 to 500 Hz frequency range frequently associated with the peak sound pressure levels quoted in the literature.

With a four-segment spectrum the peak spectral SPL at low engine speeds occurred below 200 Hz in the first or second spectral segments. However, near maximum engine speeds the peak SPL tended to shift to the third spectral segment and occurred near 500 Hz.

OVERALL SOUND PRESSURE LEVEL

Overall sound pressure levels, OASPL, at $\theta = 120^\circ$ were calculated from the measured data for the engine operating conditions given in figures 6 through 8. Good correlation of these calculated OASPL values was obtained as a function of the heat release parameter and the ratio of hydraulic-to-equivalent exhaust nozzle diameters as used in the single-segment spectrum correlation. The resultant equation is given by

$$OASPL_{\theta=120^\circ} = 100 + 10 \log w \left(\frac{P_c}{P_a} \frac{\Delta T_c}{T_{c,i}}\right)^2 \left[\left(\frac{D_h}{D_e}\right)\right]^4 - 20 \log R \qquad (16)$$

The correlated OASPL data are shown in figure 9, normalized for the distance from the core nozzle exit plane. All levels are free field plus 6dB.

The difference between the calculated and measured OASPL values is shown in figure 10 for the one-, two-, and four-segment spectra as a function of engine speed. In all cases the $OASPL_{cal}$-$OASPL_{meas}$ values are within ±3 dB. With a single-segment spectrum the differences in OASPL at engine speeds greater than 60 percent were a function of a particular engine, with plus dB values of 2 or greater for the YF102 and about -2 dB for the CF6-50 engines. The values for the JT15D engine were within ±1.2 dB. For the two and four-segment spectra these differences in this speed range were reduced to ±1 dB, except at 60-percent engine speed. In general, the 2- and 4-segment spectra are preferred for summing with other engine noise spectra (jet, shock, fan, etc.) because of their more precise spectral definition of core noise, even though the OASPL contributions for the various core noise spectra are not significantly different.

OVERALL SOUND PRESSURE LEVEL DIRECTIVITY

The variation of core noise OASPL with directivity angle for the YF102 engine is shown in figure 11 for a 30 percent engine speed. The spectral data were corrected for any obvious tones. This resulted in somewhat lower OASPL values (up to -1.8 dB) than those given in reference 8. Also shown in the figure are predicted directivities from references 4 through 6.

The OASPL variation with directivity angle is assumed not to vary significantly with engine speed. Consequently, the curve based on the three-signal coherence technique in figure 11 is believed to be directly applicable to the engines and operating conditions included herein.

FLIGHT EFFECTS

In order to project the static core noise data herein to flight, the method of reference 6 is recommended. The static-to-flight transformation is given by the following:

$$OASPL_F - OASPL_S = -40 \log (1 - M_0 \cos \theta) \qquad (17)$$

CONCLUDING REMARKS

In reference 8 it was pointed out that at the higher frequencies (above 400 Hz) the three-signal coherence technique yielded sound pressure levels that are 2 to 5 dB below those obtained by subtracting jet and fan predicted noise levels from the total measured noise. Several reasons were postulated in the reference to account for this difference. These reasons included (1) Fan noise levels were underpredicted; (2) Coherence existed between the non-radiating noise at the two engine probes; and (3) The low levels of coherence between the signals at high frequencies resulted in a bias in the core noise levels. A discussion of these items is given in the reference.

For core noise prediction the four-segment spectrum, on the basis of the available data, yields the best fit to measured spectrum obtained by the three-signal coherence technique. An acceptable fit to measured spectrum is obtained also with the simpler two-segment spectrum. Use of either spectral model for core noise prediction is considered an improvement over the methods currently available in the literature.

APPENDIX A – SYMBOLS

A_c	combustor exit area, m^2
C_a	ambient sonic velocity, m/sec
C_c	combustor exit sonic velocity, m/sec
D_c	combustor exit effective diameter
D_e	nozzle effective diameter, m
D_h	nozzle hydraulic diameter, m
f	1/3-octave band center frequency, Hz
f_p	peak segment frequency, Hz
M_o	flight Mach number, dimensionless
OASPL	overall sound pressure level, dB re 20 N/m^2
P_a	ambient pressure, N/m^2
P_c	combustor pressure, N/m^2
R	source-to-observer distance, m
SPL	sound pressure level, dB re 20 N/m^2
SPL_p	peak sound pressure level, dB re 20 N/m^2
$T_{c,i}$	combustor inlet temperature, K
ΔT_c	combustor temperature rise, K
V_c	combustor exit velocity, m/s
w	combustor mass flow rate, kg/sec
ΔdB	SPL_p – SPL, dB
ρ_a	ambient air density, kg/m^3
ρ_c	combuster exit gas density, kg/m^3
θ	directivity angle measure from the inlet, deg
Subscripts	
I, II, III, IV	spectral segments
120°	evaluation at θ = 120°

cal	calculated
F	flight
meas	measured
S	static

REFERENCES

1. U. H. von Glahn, and D. E. Groesbeck, "Comparison of Predicted Engine Core Noise with Current and Proposed Aircraft Noise Certification Requirements, "NASA TM-82659, National Aeronautics and Space Administration, Washington, D.C. (1981).

2. U. H. von Glahn, and D. E. Groesbeck, "Comparison of Predicted Engine Core Noise with Proposed FAA Helicopter Noise Certification Requirements, "NASA TM-81739, National Aeronautics and Space Administration, Washington, D.C. (1981).

3. C. G. Hodge, "Subsonic Transport Noise," AIAA Paper No. 80-0858 (May 1980).

4. R. G. Huff, B. J. Clark, and R. G. Dorsch, "Interim Prediction Method for Low Frequency Core Engine Noise, "NASA TM X-71627, National Aeronautics and Space Administration, Washington, D.C. (1974).

5. R. K. Matta, G. T. Sandusky, and V. L. Doyle, "G. E. Core Engine Noise Investigation - Low Emission Engines, "FAA-RD-77-4, General Electric Co., Cincinnati, Oh (Feb. 1977).

6. J. R. Stone, "Flight Effects on Exhaust Noise for Turbojet and Turbofan Engines - Comparison of Experimental Data with Prediction, "NASA TM X-73552, National Aeronautics and Space Administration, Washington, D.C. (1976).

7. D. C. Mathews, N. F. Rekos, Jr., and R. T. Nagel, "Combustion Noise Investigation, "PWA-5478, FAA-RD-77-3, Pratt Whitney Aircraft Group, East Hartford, Conn (1977).

8. E. A. Krejsa, "New Technique for the Direct Measurement of Core Noise from Aircraft Engines, "NASA TM-82634, National Aeronautics and Space Administration, Washington, D.C. (1981).

9. M. Reshotko, and A. Karchmer, "Core Noise Measurements from a Small General Aviation Turbofan Engine, "NASA TM-81610, National Aeronautics and Space Administration, Washington, D.C. (1980).

10. M. Reshotko, A. M. Karchmer, P. E. Penko, and J. G. McArdle, "Core Noise Measurements on a YF-102 Turbofan Engine, "NASA TM X-73587, National Aeronautics and Space Administration, Washington, D.C. (1977).

11. V. L. Doyle, and M. T. Moore, "Core Noise Investigation of the CF6-50 Turbofan Engine, "R79AEG395, General Electric Co., Cincinnati Oh (Jan. 1980).

12. R. E. Motsinger, and J. J. Emmerling, "Review of Theory and Methods for Combustion Noise Prediction," AIAA Paper No. 75-541, March, 1975.

13. M. S. Howe, "Attenuation of Sound in a Low Mach Number Nozzle Flow," J. of Fluid Mechanics, Vol. 91, Part 2, pp. 209-229, 1979.

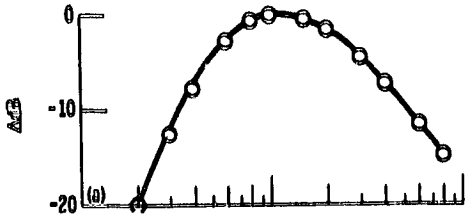

SPECTRAL COORDINATES

f/f_p	ΔdB
0.2	-20.0
.3	-12.3
.4	-7.6
.6	-2.7
.8	-0.8
1.0	0
1.5	-0.9
2.0	-1.9
3.0	-4.4
4.0	-7.0
6.0	-11.4
8.0	-14.7

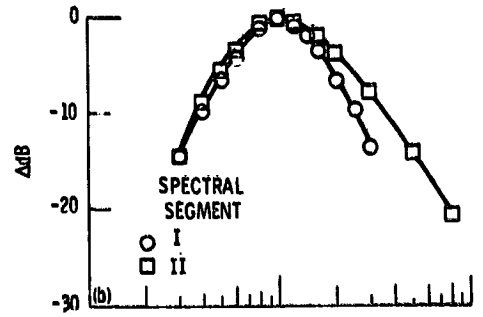

SPECTRAL COORDINATES

SEGMENT I (LOW FREQUENCY)		SEGMENT II (HIGH FREQUENCY)	
f/f_p	ΔdB	f/f_p	ΔdB
0.3	-14.8	0.3	-14.8
0.4	-9.8	.4	-8.8
.5	-6.5	.5	-5.2
.6	-4.0	.6	-3.2
.8	-1.0	.8	-0.8
1.0	0	1.0	0
1.2	-0.8	1.2	-0.7
1.4	-2.0	1.6	-2.0
1.6	-3.4	2.0	-3.8
2.0	-6.5	3.0	-7.7
2.5	-9.8	5.0	-14.0
3.0	-13.5	8.0	-20.5

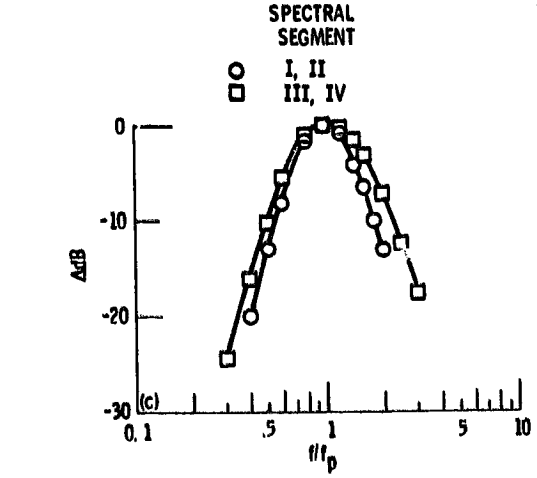

SPECTRAL COORDINATES

SEGMENTS I AND II (LOW FREQUENCY)		SEGMENTS III AND IV (HIGH FREQUENCY)	
f/f_p	ΔdB	f/f_p	ΔdB
0.4	-20.0	0.3	-24.3
0.5	-13.0	0.4	-16.0
0.6	-8.0	0.5	-10.2
0.8	-1.6	0.6	-5.5
1.0	0	0.8	-1.2
1.2	-1.0	1.0	0
1.4	-4.2	1.2	-0.5
1.6	-6.8	1.4	-1.8
1.8	-10.0	1.6	-3.1
2.0	-13.0	2.0	-7.3
		2.5	-12.4
		3.0	-17.6

(a) One-segment spectrum.
(b) Two-segment spectrum.
(c) Four-segment spectrum.

Figure 1. - Spectral coordinates.

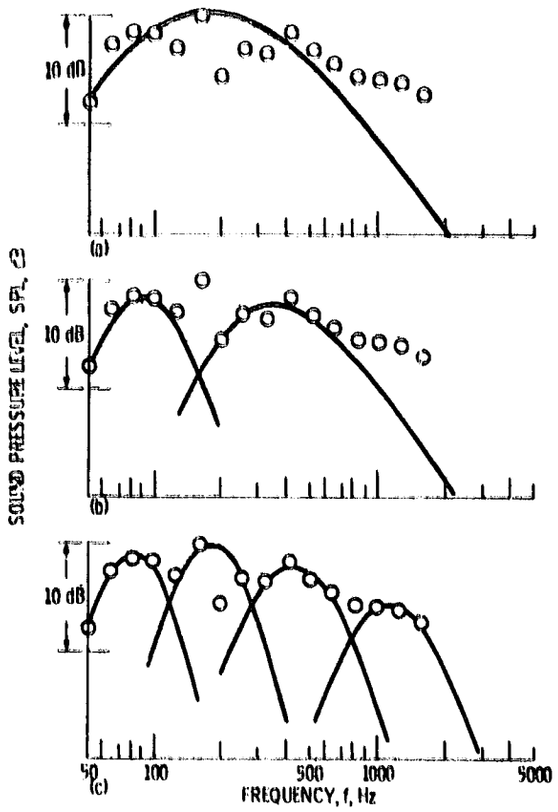

(a) One-segment spectrum.
(b) Two-segment spectrum.
(c) Four-segment spectrum.

Figure 2. - Spectral shapes applied to representative data. CF6-50 engine; 93% engine speed; θ, 120°.

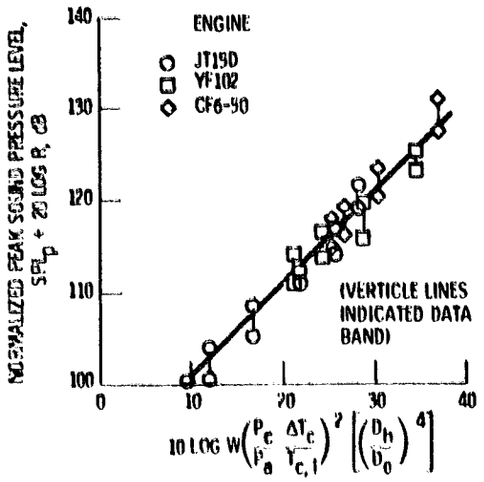

Figure 3. - Correlation of peak sound pressure level for one-segment spectrum, θ, 120°.

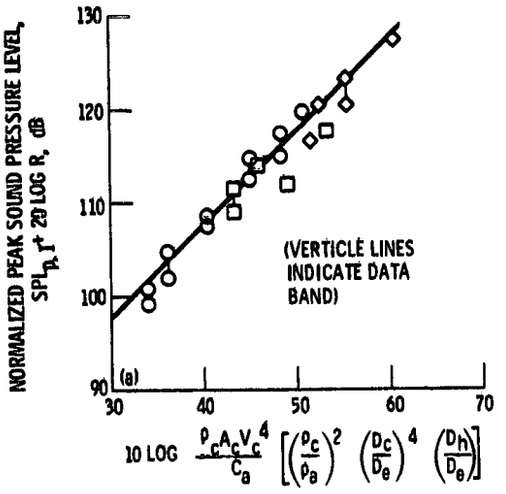

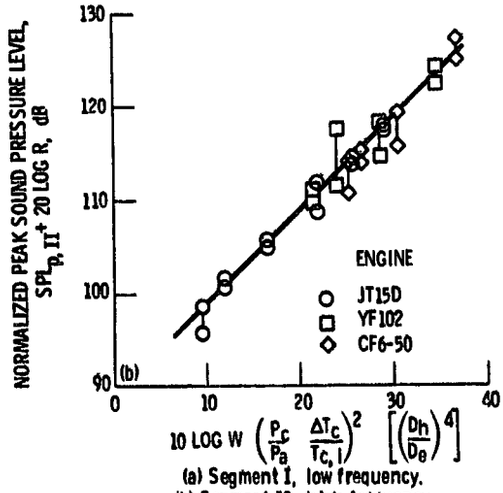

(a) Segment I, low frequency.
(b) Segment II, high frequency.

Figure 4. - Correlation of peak sound pressure level for two-segment spectrum. e, 120°.

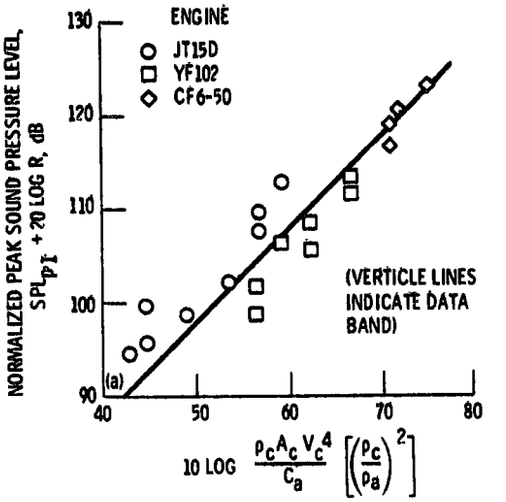

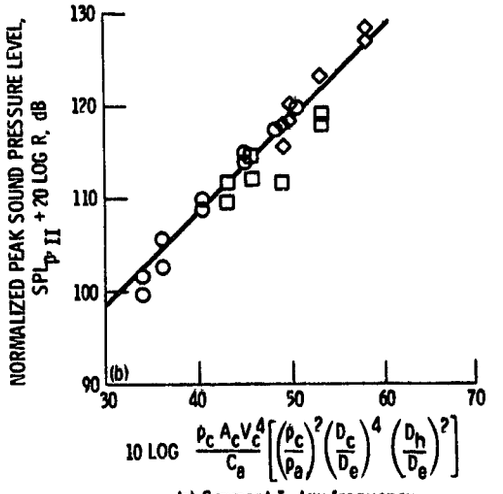

(a) Segment I, low frequency.
(b) Segment II, low frequency.

Figure 5. - Correlation of peak sound pressure level for four-segment spectrum. e, 120°.

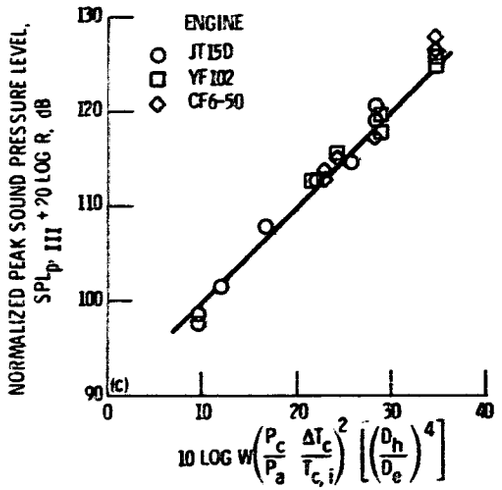

(c) Segment III, high frequency.
(d) Segment IV, high frequency.

Figure 5. - Concluded.

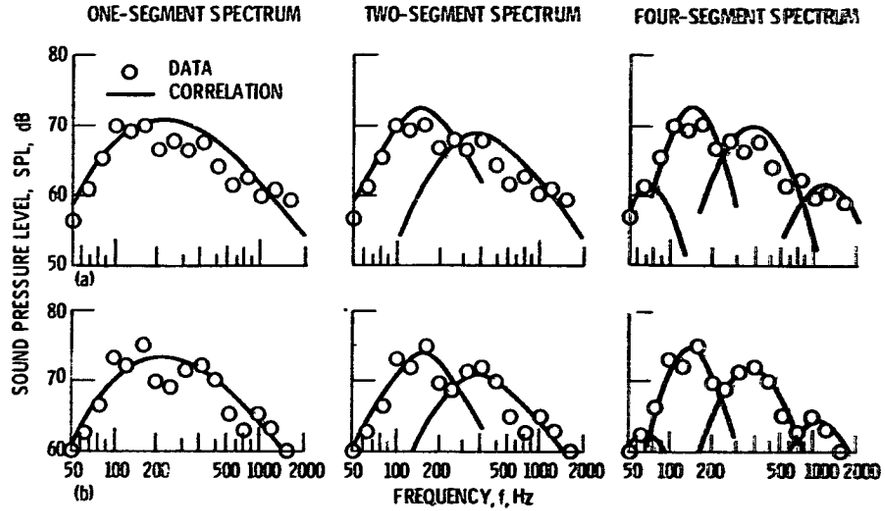

(a) 33⅓ engine speed.
(b) 40% engine speed.

Figure 6. - Comparison of measured spectra with several correlation spectra. JT15D engine; θ, 120°.

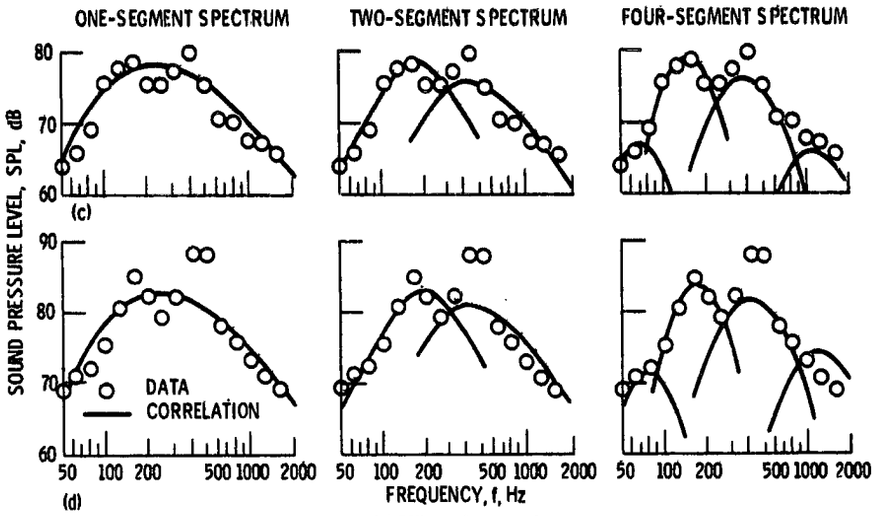

(c) 55% engine speed.
(d) 73% engine speed.

Figure 6. - Continued.

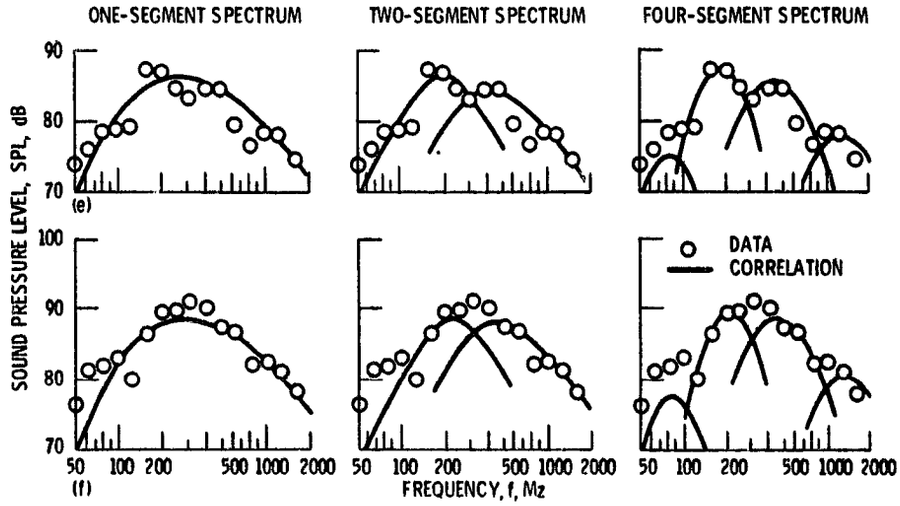

(e) 87% engine speed.
(f) 97% engine speed.

Figure 6. - Concluded.

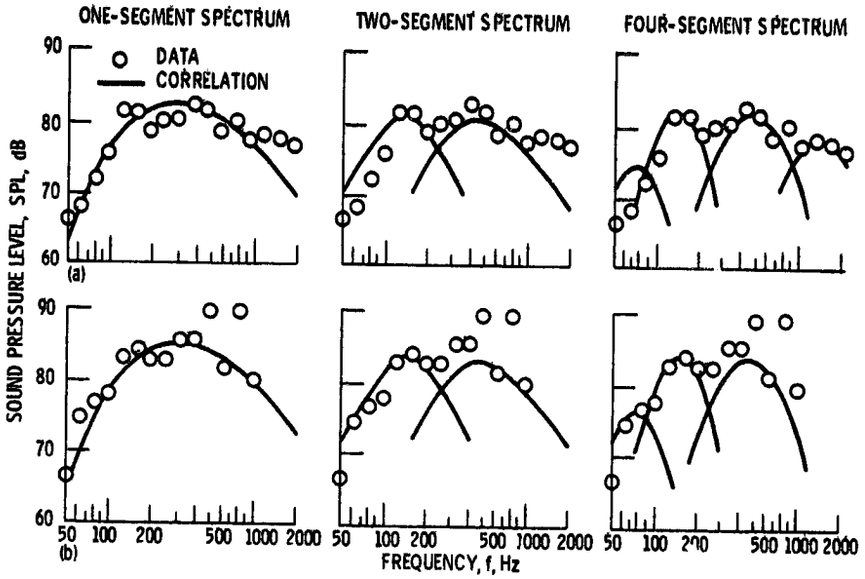

(a) 50% engine speed.
(b) 60% engine speed.

Figure 7. - Comparison of measured spectra with several correlation spectra. YF102 engine; θ, 120°.

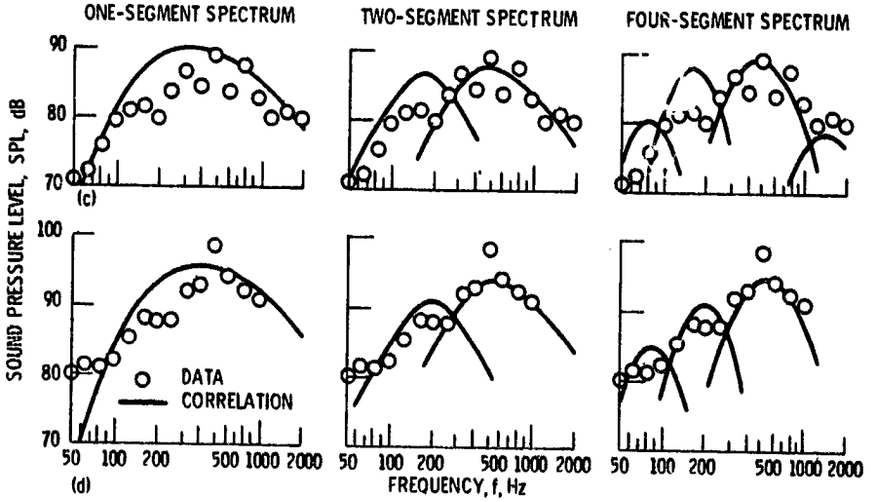

(c) 75% engine speed.
(d) 95.5% engine speed.

Figure 7. - Concluded.

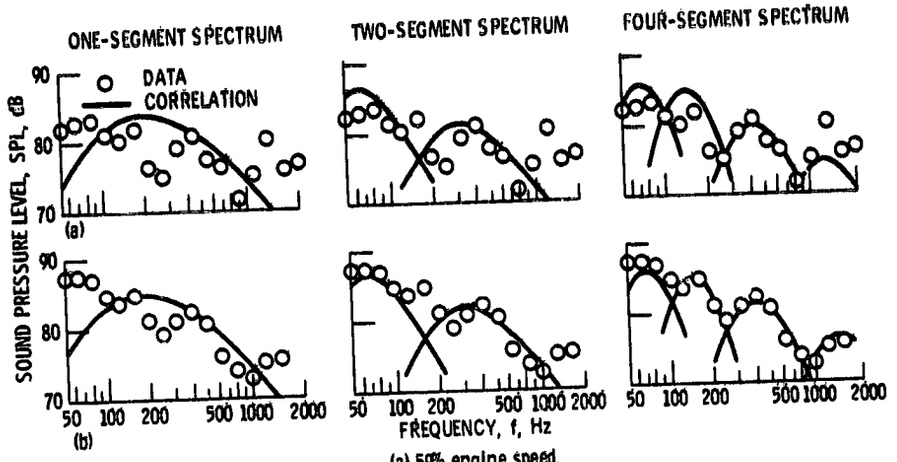

(a) 59% engine speed.
(b) 63% engine speed.

Figure 8. - Comparison of measured spectra with several correlation spectra. CF6-50 engine; θ, 120^0.

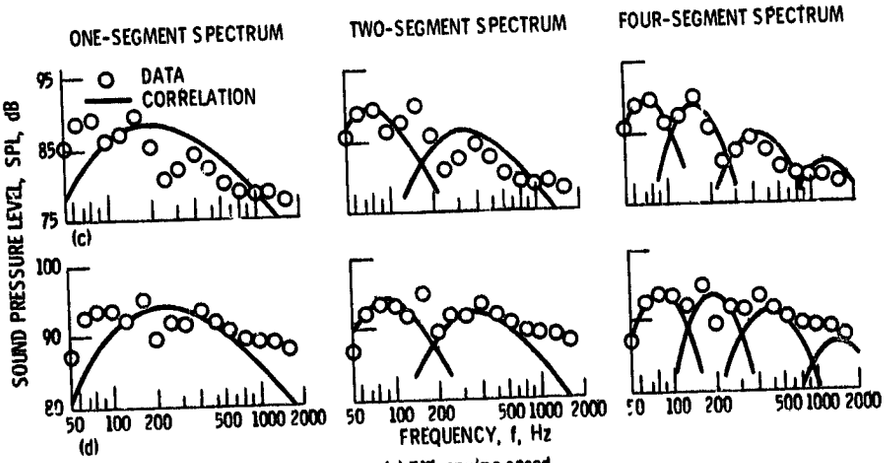

(c) 71% engine speed.
(d) 93% engine speed.

Figure 8. - Concluded.

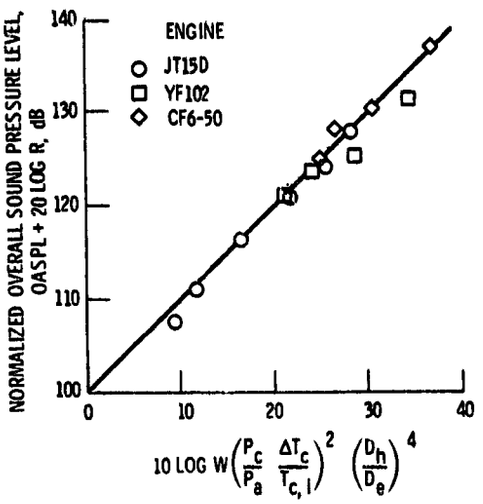

Figure 9. - Correlation of measured overall sound pressure levels with modified heat release parameter. e, 120°; distance from nozzle exit plane, 30.5 m.

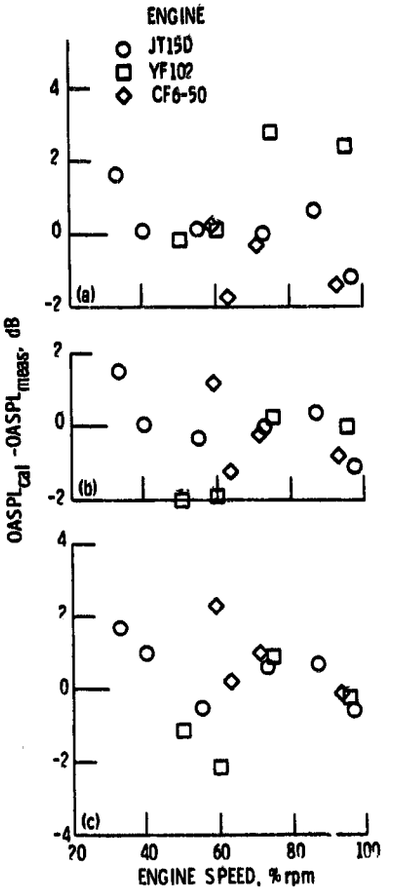

(a) One-segment spectrum.
(b) Two-segment spectrum.
(c) Four-segment spectrum.

Figure 10. - Difference between calculated and measured OASPL for various spectral segmentations as a function of engine speed. e, 120°.

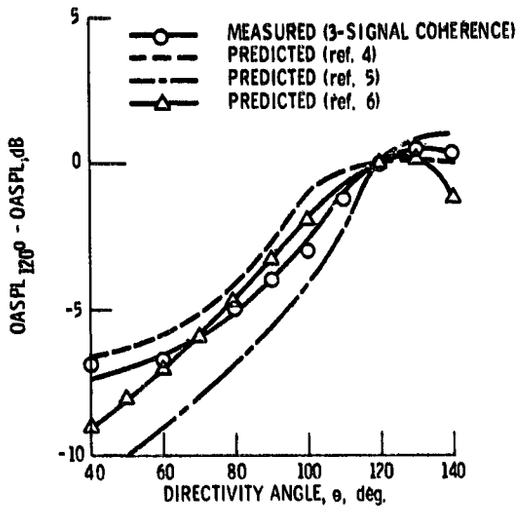

Figure 11. - Comparison of measured and predicted OASPL directivity. YF102 engine; 30% engine speed.